

Thioredoxin-1 actively maintains the pseudokinase MLKL in a reduced state to suppress disulfide bond-dependent MLKL polymer formation and necroptosis

Eduardo Reynoso¹, Hua Liu^{1,2}, Lin Li³, Anthony L. Yuan¹, She Chen³, Zhigao Wang^{1,*}

¹Department of Molecular Biology, University of Texas Southwestern Medical Center, Dallas, TX 75390, USA

²School of Pharmacy, Jiangxi University of Traditional Chinese Medicine, Nanchang, Jiangxi 102206, China

³Proteomics facility, National Institute of Biological Sciences, Beijing, 330006, China

Running title: Thioredoxin-1 suppresses MLKL polymerization and necroptosis

*Correspondence: Zhigao.wang@utsouthwestern.edu; Tel: 1-214-648-1228

Keywords: necrosis (necrotic death); serine/threonine protein kinase; thioredoxin; tumor necrosis factor (TNF); tumor therapy; RIPK3, MLKL

Abstract

Necroptosis is an immunogenic cell death program that is associated with a host of human diseases, including inflammation, infections and cancer. Receptor-interacting protein kinase 3 (RIPK3) and its substrate mixed lineage kinase domain-like protein (MLKL) are required for necroptosis activation. Specifically, RIPK3-dependent MLKL phosphorylation promotes the assembly of disulfide bond-dependent MLKL polymers that drive the execution of necroptosis. However, how MLKL disulfide bond formation is regulated is not clear. In this study, we discovered that the MLKL-modifying compound necrosulfonamide crosslinks cysteine 86 of human MLKL to cysteine 32 of the thiol oxidoreductase thioredoxin-1 (Trx1). Recombinant Trx1 preferentially binds to monomeric MLKL, and blocks MLKL disulfide bond formation and polymerization *in vitro*. Inhibition of MLKL polymer formation requires the reducing activity of Trx1. Importantly, shRNA-mediated knockdown of Trx1 promotes MLKL polymerization and sensitizes cells to necroptosis. Furthermore, pharmacological inhibition of Trx1 with compound PX-12 induces necroptosis in multiple cancer cell lines. Altogether, these findings demonstrate that Trx1 is a critical regulator of necroptosis that suppresses cell death by maintaining MLKL in a reduced inactive state. Our results further suggest new directions for targeted cancer therapy, in which thioredoxin inhibitors like PX-12 could potentially be used to specifically target cancers expressing high levels of MLKL or MLKL short isoforms.

Necroptosis shares many morphological features associated with necrosis in which cells become

swollen and eventually lose the integrity of their plasma membrane (1-3). The result is the release of intracellular damage-associated molecular patterns (DAMPs) into the surrounding tissue that alert nearby immune cells and trigger inflammation (4-6). Given these outcomes, necroptosis is considered a critical cell death mechanism of the host innate immune system. Previous reports show that certain pathogens modulate necroptosis by direct engagement of the necroptotic machinery. For example, Influenza A viral genomic RNA is sensed by DNA activator of interferon (DAI), a RIPK3-interacting protein, which in turn induces necroptosis to help mitigate infection and clear the pathogen from the organism (7,8). Conversely, Herpes Simplex Virus types 1 and 2 infection represses necroptosis by expressing RIP homotypic interacting motif (RHIM)-domain containing factors that sequester RIPK3 as a means for blocking cell death (9,10). However, like other cell death programs, dysregulated necroptosis contributes to a broad spectrum of human diseases linked to inflammation, neurodegeneration, and ischemic/reperfusion injury (11-17). Overactive necroptosis is thought to occur as a result of changes in gene expression that elevate RIPK1/3 and MLKL protein levels, although the mechanism by which these changes occurs is undefined. Consequently, cells become sensitized to necroptotic stimuli causing undesired cell death and irreversible tissue damage. Therefore, understanding the molecular mechanisms that regulate necroptosis will help advance current efforts in developing therapeutic strategies for modulating necroptosis *in vivo*, a challenge that has persisted in the field thus far.

Most of our understanding of the necroptotic machinery has emerged through studies of the TNF- α signaling pathway. These works led to the discovery of serine/threonine kinases RIPK1/3 and MLKL as critical mediators of necroptosis (18-24). Together, these proteins form the core of the necrosome complex that is central for transducing necroptotic signals. One common method for inducing necroptosis is by treating cells grown in culture with a cocktail comprised of TNF- α , a Smac-mimetic, which degrades cellular inhibitors of apoptosis (cIAPs), and the pancaspase inhibitor Z-VAD-FMK (21, 25, 26). This cocktail is abbreviated as T/S/Z. It drives necrosome complex formation and RIPK3-dependent phosphorylation of Thr357 and Ser358 located within C-terminal kinase-like domain of human MLKL (27, 28). Active MLKL molecules co-localize with various cellular compartments and interact with a specific subset of phosphatidylinositol phospholipids (PIPs) (29-34). MLKL then forms oligomers that somehow disrupt the integrity of the plasma membrane through a process that is not fully understood. Previous reports show that MLKL oligomers are stabilized by intermolecular disulfide bonds (29, 30, 35). Recently we demonstrated that MLKL forms disulfide bond-dependent amyloid-like fibers to promote necroptosis. MLKL mutant with multiple cysteine residues changed to serine residues could not form intermolecular disulfide bonds and is greatly compromised in its ability to induce necroptosis (36). These results suggest that MLKL activity is tightly regulated by its redox state. Interestingly, mitochondrial dysfunction and ROS production are observed during necroptosis (37). In murine cells, TNF- α -induced necroptosis can be prevented by co-treating cells with ROS scavenging molecules such as butylated hydroxyanisole (BHA) or N-acetylcysteine (NAC) (38). More recently, mitochondrial ROS induced RIPK1 autophosphorylation bolstering the idea that oxidation plays an important role in the mammalian necroptotic pathway (39). However, whether similar oxidative events drive MLKL activation in human cells remains a topic of much debate.

Here, we provide evidence that thioredoxin-1 (Trx1), a 12kDa thiol oxidoreductase, suppresses necroptosis by blocking MLKL disulfide bond formation and polymerization. Trx1 functions as an anti-oxidizing enzyme that is central for regulating

cellular redox balance. Trx1 protects cells from oxidative stress by catalyzing thiol disulfide exchange reactions that results in the reduction of disulfide bonds on specific protein targets, thereby modulating their activities (41, 42). Proteins regulated by Trx1 include cell surface receptors, kinases, transcription factors, and other signaling molecules that are involved in a multitude of biological processes including cell death (42-44). In this study, we found that necrosulfonamide (NSA), a small molecule inhibitor of MLKL (23), crosslinks Cys32 of Trx1 to Cys86 of human MLKL. *In vitro* interaction studies revealed that Trx1 interacts with MLKL and maintains MLKL in a reduced state. Knockdown of Trx1 by shRNA enhanced MLKL tetramer and polymer formation. Moreover, Trx1 knockdown cells were more sensitive to necroptosis upon induction of RIPK3 and MLKL protein expression. These results were further corroborated with the use of a commercially available Trx1 inhibitor, PX-12, which disables the recycling of Trx1 by thioredoxin reductase. PX-12 treatment promoted RIPK1/RIPK3/MLKL necrosome formation, RIPK3-dependent MLKL phosphorylation, MLKL polymerization, and ultimately caspase-independent necrotic cell death. Overall, these findings point to Trx1 as a suppressor of necroptosis that functions at the step of MLKL polymer formation.

Results

NSA crosslinks Cys32 of thioredoxin-1 to Cys86 of human MLKL

Necrosulfonamide (NSA) is a synthetic compound that inhibits necroptosis in human cells (23). NSA contains two potential Michael acceptors which covalently conjugate cysteine residues on target proteins. Mutation of either Michael acceptor renders NSA non-functional (23). By irreversibly conjugating Cys86 of human MLKL protein, NSA prevents necroptosis without affecting RIPK1/RIPK3/MLKL necrosome complex formation or RIPK3-dependent MLKL phosphorylation (23,27,36). We observed that NSA crosslinked MLKL to an endogenous protein in NTD-DmrB-FLAG cells, which stably express a truncated MLKL transgene containing the N-terminal domain (NTD), fused to an interaction-inducible DmrB domain under the control of a Dox-inducible promoter (Fig. 1A). Western blot analysis revealed that NSA, but not NSA-D1 produced a

prominent extra protein band that migrated near 55 kDa (lane 2 and 3, Fig. 1B), which is about 12-15 kDa larger than NTD-DmrB itself. This indicated that NSA requires two cysteine-reactive Michael acceptor moieties, one of which is lacking in NSA-D1 to successfully crosslink MLKL to a 12-15 kDa endogenous protein. As expected, NSA crosslinking required Cys86 of MLKL which is a known targeting site for NSA (lane 4, Fig. 1C).

Next, we set out to determine the identity of the protein crosslinked to NTD-DmrB by NSA. NTD-DmrB-NSA-protein complexes were isolated from whole cell extracts by FLAG-tag affinity purification, and subjected to SDS-PAGE for silver staining (Fig. 1D). The 55kDa gel band of interest was excised and subjected to LC/MS analysis to determine the protein composition. The list of candidate proteins was narrowed down to those with a molecular weight between 12-15 kDa. One of the proteins that fit this criterion was thioredoxin-1 (Trx1). Trx1 is a small cytoplasmic oxidoreductase that catalyzes the reduction of disulfide bonds on specific protein substrates. To verify that Trx1 was crosslinked to MLKL by NSA, we ectopically expressed either wild-type or a C86S mutant HA-FLAG-MLKL full-length protein in HEK293T cells, and treated these cells with NSA for 16 hours. Anti-Trx1 Western blotting of the FLAG-IP product confirmed that Trx1 was crosslinked by NSA to wild-type MLKL (Lane 2), but not to C86S mutant (lane 4) (Fig. 1E). MLKL-NSA-Trx1 crosslinking was also confirmed through ectopic expression of HA-tagged Trx1 in HeLa:GFP-RIPK3:MLKL cells, which stably express GFP-RIPK3 and MLKL-HA-FLAG under the control of a Dox-inducible promoter (Fig. 1F). In HA-Trx1 expressing cells, NSA crosslinked MLKL to both endogenous Trx1 and HA-Trx1, producing two crosslinking products (lane 4, Fig. 1F).

The ability of Trx1 to reduce disulfide bonds is attributed to two reactive cysteine residues, Cys32 and Cys35, located within its active site (40, 41). To determine which cysteine of Trx1 reacts with NSA, we mutated Cys32 and Cys35 to serine residues individually or in combination and tested MLKL crosslinking. FLAG-IP revealed that C32S, but not C35S, failed to conjugate MLKL, indicating that Cys32 is necessary for NSA crosslinking (lane 4,

Fig. 1G). This suggests that the catalytic domain of Trx1 mediates the interaction with MLKL.

Trx1 interacts with MLKL in a signal-dependent manner

Given that NSA crosslinks Trx1 to MLKL under normal conditions, we tested whether Trx1 could directly bind to MLKL in cells. However, attempts to verify their interaction by standard MLKL- or Trx1-immunoprecipitation assays were not successful. To overcome this challenge, we first immobilized recombinant HA-Trx1-6xHis purified from BL21 bacteria cells to Nickel-agarose beads, and incubated them with cell extracts prepared from HeLa:GFP-RIPK3:MLKL cells. Nickel beads containing wild-type Trx1 were able to pulldown MLKL (lane 2, Fig. 2A), which was not the case with the beads containing the C32S (C32S-C35S) mutant (lane 3, Fig. 2A). Next, immobilized Trx1 nickel beads were incubated with either control or T/S/Z-induced necroptotic cell extracts prepared from HT-29 cells (Fig. 2B and 2C). Both wild-type Trx1 and the C35S mutant bound MLKL (lane 3-6, Fig. 2C). Interestingly, C35S mutant showed even higher affinity with MLKL than wild-type (compare lane 5 and 3), similar to a previous report that C35S mutant constitutively interacted with its known substrate apoptosis signal-regulating kinase 1 (ASK1) with higher affinity (44). Importantly, Trx1 binding affinity with MLKL was significantly higher in control extracts than extracts prepared from T/S/Z treated cells (lane 3 and 4, lane 5 and 6, Fig. 2C), suggesting that Trx1 preferentially associates with monomeric MLKL molecules under normal condition.

Trx1 reduces MLKL disulfide bonds to inhibit MLKL polymer formation

Trx1 reduces disulfide bonds on specific target proteins, thereby maintaining the reducing environment of the cytoplasm, preventing undesired protein aggregation, and regulating redox signaling pathways (40, 41). Previous reports indicate that MLKL tetramers are stabilized by intermolecular disulfide bonds (29, 30, 35), which is also the case for larger MLKL polymers (36). As shown in Fig. 3A, T/S/Z treatment induced MLKL phosphorylation in HeLa:GFP-RIPK3:MLKL cells. Phosphorylated MLKL was mainly found in tetramers revealed by non-reducing SDS-PAGE (lane 2, Fig. 3B). The MLKL tetramers were

stabilized by disulfide bonds, because incubation with 5 mM beta-mercaptoethanol for 30 minutes at 30°C reduced tetramer back to the monomeric state (lane 4, Fig. 3B). Next semi-denaturing detergent agarose gel electrophoresis (SDD-AGE) was used to resolve megadalton size NLKL polymers that are resistant to SDS exposure. T/S/Z treatment resulted in MLKL polymer formation (lane 2, Fig. 3C), which were dissociated after incubation with 5 mM DTT for 30 minutes at 30°C (lane 4, Fig. 3C). Altogether, these results confirm that active MLKL tetramers and polymers are stabilized by disulfide bonds.

To address the mechanism by which Trx1 regulates MLKL function, we employed a cell-free system that was recently reported (36) to assess MLKL polymerization *in vitro*. Recombinant GST-NTD-FLAG protein was purified from BL21 bacteria cells. Overnight incubation of GST-NTD-FLAG at 37°C resulted in MLKL polymer formation (lane 2, Fig. 3D). Importantly, GST-NTD incubated at 4°C did not polymerize suggest that the process is temperature sensitive (lane 1). Moreover, incubating polymers with DTT resulted in total dissociation of the polymers (lane 3, Fig. 3D), confirming the importance of disulfide bond formation for *in vitro* MLKL polymerization. To test the effect of Trx1 in this system, 5 μ M GST-NTD-FLAG protein was incubated with increasing amounts of recombinant Trx1 (3 μ M, 10 μ M, and 30 μ M) overnight at 37°C. Wild-type Trx1 inhibited MLKL tetramer formation in a dose-dependent manner (lane 2-4) while the CS2 mutant did not (lane 5-7, upper panel, Fig. 3E). Similarly, wild-type Trx1 but not CS2 mutant blocked MLKL polymer formation (upper panel, Fig. 3F), suggesting that the Trx1 reductase activity is required to keep MLKL in a monomeric state. Protein levels of recombinant GST-NTD-FLAG and HA-Trx1-6xHis in the reaction were visualized by Coomassie Blue staining (lower panel, Fig. 3F). These results confirm that MLKL is a substrate of Trx1 and Trx1 maintains MLKL in a reduced monomeric state *in vitro* to prevent MLKL polymerization.

shRNA-mediated Trx1 knockdown promotes MLKL polymerization and sensitizes cells to necroptosis Trx1 is an essential gene, and therefore cannot be successfully knocked out in cells (45). In

order to overcome this challenge and test whether Trx1 suppresses MLKL activation, we stably introduced a Dox-inducible Trx1 shRNA cassette into the genome of HeLa:GFP-RIPK3:MLKL cells by lentiviral transduction (Fig. 4A). shTrx1 cells grew at similar rates as parental cells, and exhibited normal morphology. After 72 hours of Dox treatment, cell extracts from parental and shTrx1 cells were collected and probed for Trx1, RIPK3, and MLKL protein levels by Western blotting. Dox treatment induced GFP-RIPK3 and MLKL expression (lane 2 and 4, Fig. 4A), and greatly reduced Trx1 expression by shTrx1 (lane 4, Fig. 4A). Notably, even without Dox, Trx1 expression was already reduced (lane 3), suggesting the occurrence of leaking shRNA expression. Inhibition of Trx1 is known to activate apoptosis signal regulating kinase 1 (ASK1) to induce apoptosis (43, 44). Therefore, to eliminate Trx1 reduction induced apoptosis effect, Z-VAD-FMK was included in all the analysis for Trx1 knockdown or inhibition experiments. Next, cell extracts were subjected to non-reducing SDS-PAGE analysis to test whether knockdown of Trx1 promoted MLKL tetramer formation. Indeed cells with diminished levels of Trx1 presented higher amounts of MLKL tetramers (lane 4, Fig. 4B). Moreover, MLKL polymers were also detected by SDD-AGE in Trx1 knockdown samples (lane 4, Fig. 4C). Lastly, cell death measurement indicated that reduction of Trx1 protein resulted in significantly higher sensitivity to necroptosis (column 2 and 4, Fig. 4D). These results suggest that Trx1 functions to keep MLKL in a reduced state to suppress MLKL polymerization and activation (Fig. 4E).

To address the possibility that the crosslinking product MLKL-NSA-Trx1 might contribute to NSA's ability to block cell death, we tested the effect of NSA in shTrx1 cells. In cells that had reduced levels of Trx1, MLKL-NSA-Trx1 was not detectable (lane 4, Fig. 4F). However, NSA was fully capable to block T/S/Z induced cell death (column 5 and 6, Fig. 4G), suggesting that the crosslinking product MLKL-NSA-Trx1 is not required for NSA to block necroptosis. This confirms our previous result that NSA could directly block MLKL polymerization *in vitro* (36).

Trx1 inhibitor PX-12 induces necroptosis in HeLa:GFP-RIPK3:MLKL cells

Since Trx1 knockdown sensitized cells to necroptosis, we tested if chemical inhibition of Trx1 activity exhibited the same effect. This could have significant implication in cancer biology, since induction of necroptosis in tumors could potentially enhance immune response to cancer cells resulting in heightened anti-tumor immunity (46, 47). Therefore, we employed a commercially available Trx1 inhibitor PX-12, which irreversibly binds to Cys73 of Trx1, and prevents its two active site cysteines from being reduced by Thioredoxin Reductase (48). We first tested PX-12 effect in HeLa:GFP-RIPK3:MLKL cells, which express RIPK3 and MLKL transgenes under the control of a Dox-inducible promoter (lane 2, Fig. 4A). Cells were treated with or without Dox for 24 hours followed by treatment with Z-VAD-FMK and increasing amount of PX-12 ranging from 3 μ M to 30 μ M for additional 16 hours. Cells with Dox treatment exhibited significantly higher sensitivity to PX-12 than those that were not given Dox (Fig. 5A). At 10 μ M, PX-12 induced about 60% cell death (column 8), similar to the effect of T/S/Z (column 10). Importantly, co-treatment with NSA rescued PX-12-induced cell death, confirming the involvement of MLKL (column 13, Fig. 5A). We also stained the cells with the cell-impermeable DNA dye SYTOX Green. This confirmed that the observed cell death in PX-12/Z treatment is likely necroptosis and not apoptosis (Fig. 5B).

After determining that RIPK3-MLKL expression sensitized cells to PX-12-induced cell death, we evaluated the status of canonical biomarkers of necroptosis. PX-12 treatment induced MLKL phosphorylation at a putative RIPK3-specific phosphorylation site, S358, indicating that RIPK3 kinase activity was positively stimulated during PX-12-induced cell death (lane 2 of Input, Fig. 5C). Next, we performed a FLAG-IP and detected RIPK1, RIPK3, and MLKL recruitment to the necrosome complex after PX-12/Z treatment (lane 2, Fig. 5C). Moreover, PX-12 induced MLKL tetramer (lane 2 and 5, Fig. 5D) and polymer formation (lane 2, Fig. 5E), demonstrated by non-reducing SDS-PAGE and SDD-AGE, respectively. Taken together, Trx1 inhibition by PX-12 led to necrosome formation, MLKL polymerization and necroptosis (Fig. 5F).

PX-12 induces RIPK3-independent necroptosis in NTD-DmrB cells.

Many cancer cells do not express RIPK3, including HeLa cells (21). To expand the potential usage of PX-12 in anti-cancer therapy, we tested PX-12 in NTD-DmrB-FLAG cells, which are generated in a HeLa cell background. We have shown previously that addition of Dimerizer is sufficient to induce the homo-interaction of the DmrB domain, which leads to MLKL polymerization and ultimately necroptosis (36) (left panel, Fig. 6A). To test whether the expression of NTD-DmrB sensitized cells to necroptosis after PX-12 treatment, we treated cells with or without Dox for 24 hours followed by increasing concentrations of PX-12 (1 μ M-10 μ M) in combination with Z-VAD-FMK for additional 16 hours. Cell death was measured by CellTiter-Glo assay. Cells expressing NTD-DmrB were significantly more sensitized to PX-12-induced cell death, which could be blocked by co-treatment with NSA (Compare column 4, 9 and 14, Fig. 6A). Cell death was confirmed to be necrotic in nature by SYTOX Green staining (Fig. 6B). PX-12 also appeared to stabilize NTD-DmrB, and promoted the formation of tetramers and high molecular weight polymers (lane 2, Fig. 6C and 6D, respectively). These results suggest that inhibition of Trx1 can induce necroptosis in a RIPK3-independent manner by directly promoting MLKL polymerization (Fig. 6E).

Discussion

Necroptosis has garnered increasing attention over the past several years for its implications in host immune defense and disease. At the heart of the necroptotic pathway is RIPK1, RIPK3 and MLKL, the major components of the necrosome complex. In mammalian cells, RIPK3-dependent MLKL activation leads to the formation of lethal MLKL polymers (36). Current models of necroptosis indicate that MLKL polymers are responsible for disrupting the integrity of the plasma membrane. MLKL polymers were previously shown to be stabilized by intermolecular disulfide bonds as reducing agents such as DTT and β -mercaptoethanol readily dissociate oligomers and polymers *in vitro* (29, 30, 36). Yet, the mechanistic details as to how these polymers are formed remains unresolved. Herein, we identified Trx1, a thiol oxidoreductase, as a MLKL binding partner.

As depicted in our model in Fig. 4E, Trx1 interacts with MLKL under normal conditions, and actively maintains MLKL in a reduced inactive state. When the necroptotic signal comes, MLKL is recruited to the necrosome and dissociates from Trx1. This is demonstrated by the observation that Trx1 interaction with MLKL decreased significantly in T/S/Z-treated cell extracts (Fig. 2C). Within the necrosome, RIPK1 and RIPK3 form large polymers and recruit many copies of MLKL. Phosphorylation of MLKL by RIPK3 leads to MLKL conformational changes, which allow locally concentrated MLKL to form intermolecular disulfide bonds. Without the reducing power of Trx1, disulfide bond-linked MLKL tetramers further polymerize to form amyloid-like polymers to induce necroptosis.

Interestingly, only a fraction of total MLKL was crosslinked to Trx1 (Fig. 1B and 1C), suggesting that the majority of MLKL is not associated with Trx1 at any given time. One explanation is that the interaction between Trx1 and MLKL may be transient, which is common among an enzyme and its substrates. Previous reports indicate that the associations between Trx1 and its substrates are relatively weak and short-lived, particularly during oxidative stress. For example, Trx1 maintains apoptosis signal-regulating kinase 1 (ASK1) in a reduced, inactive state under normal conditions; however, increased oxidative-stress dissociates Trx1-ASK1 and induces apoptosis (43, 44). Therefore, NSA may be primarily trapping Trx1 molecules that come into contact with MLKL intermittently, which may explain why we were not able to co-immunoprecipitate Trx1 with MLKL using standard IP assays. As shown in Fig. 2, this problem was overcome by increasing the amount of available Trx1 using recombinant protein. Trx1 immobilized nickel beads were able to pulldown endogenous MLKL from HT29 cell extracts. Notably, Trx1 preferentially bound monomeric MLKL suggesting that active MLKL polymers have a lower affinity for Trx1 binding (Fig. 2C). Thus, recruitment into necrosome and subsequent alterations in MLKL conformation, potentially via RIPK3-dependent phosphorylation, may lead to Trx1-MLKL dissociation. To better understand this phenomenon, further analysis is required to determine the precise conformational changes in MLKL that affect Trx1 binding.

Mitochondrial dysfunction and ROS production has been observed during necroptosis leading researchers to hypothesize that oxidation plays an important role during necroptosis (37, 38). For instance, RIPK1 was recently shown to be activated by ROS generated during TNF- α -induced necroptosis in L929 murine cells (39). Here, we demonstrate that Trx1 directly exerts its oxidoreductase activity on MLKL to suppress necroptosis. This is supported by our findings that genetic and pharmacological inhibition of Trx1 enhanced MLKL activation as seen by polymer formation, resulting in higher sensitivity to necroptosis. The extent of necroptosis induced by Trx1 inhibition highly correlates with MLKL expression level. As shown in Figure 5 and Figure 6, PX-12 leads to much higher level of necroptosis when MLKL expression is induced with Dox treatment. Interestingly, NTD-DmrB-FLAG cells are as sensitive to PX-12 treatment as the HeLa:GFP-RIPK3:MLKL cells, even though NTD-DmrB-FLAG cells do not express RIPK3 and the expression level of NTD-DmrB transgene is about 5 times lower than MLKL-HA-FLAG (data not shown). We believe this is because the NTD-DmrB protein does not contain the auto-inhibitory C-terminal kinase-like domain, which renders it more sensitive to necroptotic signals than the full-length protein. Although NTD-DmrB is an artificially constructed transgene, there are short isoforms of MLKL that exist in nature, such as NP_001135969.1 (263aa) and XP_011521238 (293aa), which have truncated C-terminal kinase-like domain. It is conceivable that inhibition of Trx1 with PX-12 could potentially induce these short isoforms to polymerize and activate necroptosis (right panel, Fig. 6E).

Overall, these findings provide a deeper understanding of the regulatory networks that control MLKL activation. This is the first line of evidence to implicate Trx1 as a binding partner and suppressor of MLKL in cells. Reports linking Trx1-inhibition to apoptosis in cells is well established (42-44), however, our results expand cell death outcomes induced by Trx1 inhibition to necroptosis. Future studies will be directed towards whether Trx1 inhibition induces necroptosis in tissues.

A new concept in cancer immune therapy is to induce necroptosis in tumors to enhance immune response against cancer cells leading to heightened anti-tumor effect (46, 47). The notion that inhibition of Trx1 with PX-12 sensitizes some cells to necroptosis could have significant implication in that regard. So far PX-12 has been mainly used to trigger apoptosis in cancer cells (49). However, it did not show significant efficacy in multiple clinical trials (50, 51). Our data point to a new direction for cancer treatment with PX-12, which is to induce necroptosis in tumors with elevated MLKL level or with MLKL short isoforms expression. Specifically targeting these cancer patients will potentially result in better outcome with PX-12 treatment.

Materials and Methods

General Reagents

Recombinant TNF- α , Smac-mimetic and anti-human RIPK3 were prepared as described before (21). The following reagents and antibodies were used: Z-VAD-FMK (ApexBio), Necrostatin-1 (Calbiochem), Necrosulfonamide (Millipore), Dimerizer (Clontech, 635058), anti-Flag M2 antibody and affinity gel (Sigma), anti-human MLKL (Genetex, GTX107538), anti-phospho-MLKL S358 (Abcam, ab187091), anti-RIPK1 (BD, 551042), anti-LDH (Abcam, ab53292). The amount of reagents were used as following, 20 ng/ml TNF, 100 nM Smac-mimetic, 20 μ M Z-VAD-FMK, 20 nM Dimerizer, and 5 μ M NSA. . Generally, cells were treated for 16 hours for cell death analysis. For cell lysates used for Western blotting, SDD-AGE or immunoprecipitation, cells were treated for 6 hours before harvesting.

Cell Culture and Stable Cell Lines

HT-29, and HeLa cells were cultured in DMEM (high glucose) supplemented with 10% fetal bovine serum. All the HeLa stable lines were generated in the background of previously reported HeLa-TetR cells which expressed the Tet repressor (TetR) (26). (1) MLKL knockout HeLa line. MLKL knockout in the HeLa-TetR background was generated according to the protocol described in Cong et al., 2013 (52). Briefly, oligo targeting human MLKL with the sequence GCTGCCCTGGAGGAGGCTAATGG was cloned into the gRNA vector. It was cotransfected with Cas9 expressing vector into HeLa-TetR cells.

MLKL knockout was confirmed by Western blotting and sequencing. (2) NTD-DmrB-FLAG line. Amino acids 1-190 of Human MLKL fused to the DmrB domain with a C-terminal 3xFlag was driven by a Tet inducible promoter. This construct was stably integrated in the MLKL knockout HeLa cells. (3) HeLa:GFP-RIPK3:MLKL line. Tet inducible GFP-RIPK3 and Tet inducible MLKL-HA-3xFlag were stably expressed in the MLKL knockout HeLa cells. For Dox inducible expression, 50 ng/ml Doxycycline was added for 24 hours.

Mass spectrometric analysis

Mass spec analysis was done as described before (23). Briefly, protein band was excised and destained and reduced, followed by in gel trypsin digestion. The peptides were extracted and analyzed by a QSTAR XL mass spectrometer (AB Sciex, CA, USA).

Transfection

Polyjet (SigmaGen Laboratories) was used for transfection according to the manufacturer's protocol. 1×10^6 cells were seeded in 10 cm dishes 24 hours before transfection. Cells were harvested 48 hours later.

Protein Extraction and Western blotting

Cells were scraped and washed in ice-cold PBS prior to lysing them in Protein Extraction Buffer (PEB) comprised of 20mM Tris pH7.4, 150mM NaCl, 0.5% Triton X-100, 10% glycerol, and freshly added protease and phosphatase inhibitors. Cells were rotated at 4°C for 15 minutes before centrifugation at 20,000xg for 20 minutes to clear out insoluble debris. Protein concentrations were determined by Coomassie Plus Protein Assay Reagent (Thermo Scientific). Samples were boiled in 5X SDS sample buffer (250 mM Tris pH6.8, 5% beta-mercaptoethanol, 0.02% bromophenol Blue, 30% glycerol, 10% SDS) for 5 minutes, resolved by SDS-PAGE, and transferred onto PVDF membranes (Bio-Rad). Membranes were incubated in 5% Blotting-Grade Blocker (Bio-Rad) reconstituted in phosphate buffered saline (PBS) solution with 0.1% Tween-20 (PBS-T). Primary and secondary HOURSP antibodies were also diluted in 5% PBS-T milk solution.

Immunoprecipitation assay

Protein samples were diluted to a final concentration of 1 mg/mL in 1 mL of PEB and incubated with 10 μ L FLAG (M2)-agarose beads (Sigma-Aldrich), and rotated overnight at 4°C. M2-beads were washed with 1mL ice-cold extraction buffer 3 times, and directly boiled in 1X SDS sample buffer. Silver staining was performed using ProteoSilver Plus Silver Stain kit (Sigma Aldrich).

Cell Survival Assay

Cell survival was measured using CellTiter-Glo Luminescent Cell Viability Assay according to the manufacturer's protocol (Promega). Cells were seeded at 2×10^3 cells/well in white flat-bottom 96-well plates (Corning) 24 hours prior to treatment. Luminescence was measured using a BioTek Synergy 2 plate reader.

Semi-Denaturing Detergent Agarose Gel Electrophoresis (SDD-AGE)

SDD-AGE gels were made using TAE buffer (40 mM Tris, pH 8.6, 20 mM acetate, 1 mM EDTA) containing 1% agarose and 0.1% SDS. Protein samples were mixed with 4X sample buffer (2X TAE buffer, 20% glycerol, 8% SDS) at room temperature, and run at a constant 60V for 5 hours in TAE buffer containing 0.1% SDS. Proteins were transferred onto PVDF membranes by capillary action using TBS buffer (20mM Tris pH7.4, 150mM NaCl). Membranes were treated in accordance with the Western blotting procedure.

Protein Purification

Recombinant proteins were purified from Rosetta DE3 bacterial cells grown in LB media. Cultures were grown at 37°C to an O.D.600 of 0.6, then shifted to 18°C, and allowed to induce expression with 0.1mM IPTG for 16 hours. The bacteria were pelleted by centrifugation at 3,000xg for 10 minutes, washed once in ice-cold PBS and repelleted before being resuspended in 40 mL binding buffer. For HA-Trx1-6xHis, binding buffer contained 20mM Tris pH8.0, 150mM NaCl, 0.1% Triton X-100, 10% glycerol, 20mM imidazole, 10 mM beta-mercaptoethanol, 1mM PMSF, EDTA-free protease inhibitor cocktail. Cells were lysed by sonication pulsing 15 times for 30 seconds each time. Lysates were centrifuged at 10,000xg for 20 minutes and filtered before incubation with 100 μ L Ni-NTA agarose beads (Qiagen). Binding was performed at 4°C for 30 minutes. Nickel beads were

washed 3 times in binding buffer lacking beta-mercaptoethanol and eluted with binding buffer containing 250 mM imidazole. 100 μ L fractions were collected and dialyzed against PBS.

For recombinant GST-NTD-FLAG, 100 μ L Glutathione agarose beads (Pierce) were used with binding buffer containing 20mM Tris pH7.4, 150mM NaCl, 0.1% Triton X-100, 10% glycerol, 5mM DTT, 1mM PMSF, EDTA-free protease inhibitor cocktail. GST-NTD-FLAG was eluted in 100 μ L fractions with binding buffer containing 10mM reduced L-glutathione and dialyzed against PBS.

Cell staining

Cells were seeded at 1×10^5 cells/well in a 12-well plate (Cellstar). SYTOX Green and Hoechst dyes were added directly to culture media at 1 μ M and incubated for 10 minutes prior to imaging with a BioTek Cytation 3 plate reader.

In vitro GST-NTD-FLAG polymerization assay

Recombinant GST-NTD-FLAG was used at a final concentration of 5 μ M in 20 μ L of PBS. HA-Trx1-6xHis was used at a final concentration of 3 μ M, 10 μ M, and 30 μ M. To induce polymerization, samples were incubated at 37°C for 16 hours and 50 ng of GST-NTD-FLAG was used for SDD-AGE.

Trx1 shRNA knockdown

Trx1 shRNA was cloned into a modified pSuperior-puro (Oligoengine) vector. The Dox-inducible shTrx1 cassette was then subcloned into a lentiviral transfer vector containing Hygromycin resistant gene (Addgene). Lentivirus was produced by transfecting HEK293T cells with Trx1-shRNA viral vector, pMD2.G, and psPAX2 vectors in a 10 cm plate. Lentiviral media was collected at 48 hours and 72 hours post-transfection, filtered through a 0.45 μ m sterile filter, and stored at -80°C. Lentiviral transduction of HeLa:GFP-RIPK3:MLKL cells was performed by seeding cells at 1×10^5 cells/well in a 6-well plate. Cells were provided with 1 mL complete media with 1 mL of lentiviral media supplemented with 5 μ g/mL polybrene. The following day, cells were trypsinized and seeded at 1×10^5 cells/well in a 6-well plate with media containing 0.2 μ g/mL Hygromycin B. Surviving cells were expanded, and utilized for downstream

experiments after validating Trx1 knockdown. The Trx1 shRNA sense strand primer sequence is as following:

GATCCCCGTGTGAAGTCAAATGCATGTTCA
AGAGACATGCATTTGACTTCACACTTTTTA.

Acknowledgement

We thank Dr. Xiaodong Wang for compound NSA-D1, Dr. James Chen for lentiviral transfer vector and Hong Yu for excellent technical assistance. This work is supported by the Welch Foundation (I1827), and F31 fellowship to E.N. (GM111049-01A1). Z.W. is the Virginia Murchison Linthicum Scholar in Medical Research and a Cancer Prevention and Research Institute of Texas Scholar (R1222).

conflict of interest

The authors declare no conflict of interest.

Author contributions

E.R. designed, performed the experiments and wrote the paper. H.L. and A.L.Y. performed experiments in Figure 1. L.L. and S.C. performed the mass spec analysis. Z.W. designed the experiments and revised the paper.

References

1. Galluzzi, L., Vitale, I., Abrams, J. M., Alnemri, E. S., Baehoursecke, E. H., Blagosklonny, M. V., Dawson, T. M., Dawson, V. L., El-Deiry, W. S., Fulda, S., Gottlieb, E., Green, D. R., Hengartner, M. O., Kepp, O., Knight, R. A., Kumar, S., Lipton, S. A., Lu, X., Madeo, F., Malorni, W., Mehlen, P., Nunez, G., Peter, M. E., Piacentini, M., Rubinsztein, D. C., Shi, Y., Simon, H. U., Vandenabeele, P., White, E., Yuan, J., Zhivotovsky, B., Melino, G., and Kroemer, G. (2012) Molecular definitions of cell death subroutines: recommendations of the Nomenclature Committee on Cell Death 2012. *Cell Death Differ* **19**, 107-120
2. Choursistofferson, D. E., and Yuan, J. (2010) Necroptosis as an alternative form of programmed cell death. *Curr Opin Cell Biol* **22**, 263-268
3. Krysko, D. V., Vanden Berghe, T., D'Herde, K., and Vandenabeele, P. (2008) Apoptosis and necrosis: detection, discrimination and phagocytosis. *Methods* **44**, 205-221
4. Chan, F. K., Luz, N. F., and Moriwaki, K. (2015) Programmed necrosis in the cross talk of cell death and inflammation. *Annu Rev Immunol* **33**, 79-106
5. Mocarski, E. S., Guo, H., and Kaiser, W. J. (2015) Necroptosis: The Trojan horse in cell autonomous antiviral host defense. *Virology* **479-480**, 160-166
6. Kaczmarek, A., Vandenabeele, P., and Krysko, D. V. (2013) Necroptosis: the release of damage-associated molecular patterns and its physiological relevance. *Immunity* **38**, 209-223
7. Upton, J. W., Kaiser, W. J., and Mocarski, E. S. (2012) DAI/ZBP1/DLM-1 complexes with RIP3 to mediate virus-induced programmed necrosis that is targeted by murine cytomegalovirus vIRA. *Cell Host Microbe* **11**, 290-297
8. Thapa, R. J., Ingram, J. P., Ragan, K. B., Nogusa, S., Boyd, D. F., Benitez, A. A., Sridharan, H., Kosoff, R., Shubina, M., Landsteiner, V. J., Andrade, M., Vogel, P., Sigal, L. J., tenOever, B. R., Thomas, P. G., Upton, J. W., and Balachandran, S. (2016) DAI Senses Influenza A Virus Genomic RNA and Activates RIPK3-Dependent Cell Death. *Cell Host Microbe* **20**, 674-681
9. Wang, X., Li, Y., Liu, S., Yu, X., Li, L., Shi, C., He, W., Li, J., Xu, L., Hu, Z., Yu, L., Yang, Z., Chen, Q., Ge, L., Zhang, Z., Zhou, B., Jiang, X., Chen, S., and He, S. (2014) Direct activation of RIP3/MLKL-dependent necrosis by herpes simplex virus 1 (HSV-1) protein ICP6 triggers host antiviral defense. *Proc Natl Acad Sci U S A* **111**, 15438-15443
10. Huang, Z., Wu, S. Q., Liang, Y., Zhou, X., Chen, W., Li, L., Wu, J., Zhuang, Q., Chen, C., Li, J., Zhong, C. Q., Xia, W., Zhou, R., Zheng, C., and Han, J. (2015) RIP1/RIP3 binding to HSV-1 ICP6 initiates necroptosis to restrict virus propagation in mice. *Cell Host Microbe* **17**, 229-242

11. Duprez, L., Takahashi, N., Van Hauwermeiren, F., Vandendriessche, B., Goossens, V., Vanden Berghe, T., Declercq, W., Libert, C., Cauwels, A., and Vandenabeele, P. (2011) RIP kinase-dependent necrosis drives lethal systemic inflammatory response syndrome. *Immunity* **35**, 908-918
12. Linkermann, A., Brasen, J. H., De Zen, F., Weinlich, R., Schwendener, R. A., Green, D. R., Kunzendorf, U., and Krautwald, S. (2012) Dichotomy between RIP1- and RIP3-mediated necroptosis in tumor necrosis factor- α -induced shock. *Mol Med* **18**, 577-586
13. Re, D. B., Le Verche, V., Yu, C., Amoroso, M. W., Politi, K. A., Phani, S., Ikiz, B., Hoffmann, L., Koolen, M., Nagata, T., Papadimitriou, D., Nagy, P., Mitsumoto, H., Kariya, S., Wichterle, H., Henderson, C. E., and Przedborski, S. (2014) Necroptosis drives motor neuron death in models of both sporadic and familial ALS. *Neuron* **81**, 1001-1008
14. Xu, Y., Ma, H., Shao, J., Wu, J., Zhou, L., Zhang, Z., Wang, Y., Huang, Z., Ren, J., Liu, S., Chen, X., and Han, J. (2015) A Role for Tubular Necroptosis in Cisplatin-Induced AKI. *J Am Soc Nephrol* **26**, 2647-2658
15. Meng, L., Jin, W., and Wang, X. (2015) RIP3-mediated necrotic cell death accelerates systematic inflammation and mortality. *Proc Natl Acad Sci U S A* **112**, 11007-11012
16. Ofengeim, D., Ito, Y., Najafov, A., Zhang, Y., Shan, B., DeWitt, J. P., Ye, J., Zhang, X., Chang, A., Vakifahmetoglu-Norberg, H., Geng, J., Py, B., Zhou, W., Amin, P., Berlink Lima, J., Qi, C., Yu, Q., Trapp, B., and Yuan, J. (2015) Activation of necroptosis in multiple sclerosis. *Cell Rep* **10**, 1836-1849
17. Ito, Y., Ofengeim, D., Najafov, A., Das, S., Saberi, S., Li, Y., Hitomi, J., Zhu, H., Chen, H., Mayo, L., Geng, J., Amin, P., DeWitt, J. P., Mookhtiar, A. K., Florez, M., Ouchida, A. T., Fan, J. B., Pasparakis, M., Kelliher, M. A., Ravits, J., and Yuan, J. (2016) RIPK1 mediates axonal degeneration by promoting inflammation and necroptosis in ALS. *Science* **353**, 603-608
18. Holler, N., Zaru, R., Micheau, O., Thome, M., Attinger, A., Valitutti, S., Bodmer, J. L., Schneider, P., Seed, B., and Tschopp, J. (2000) Fas triggers an alternative, caspase-8-independent cell death pathway using the kinase RIP as effector molecule. *Nat Immunol* **1**, 489-495
19. Degterev, A., Hitomi, J., Gernscheid, M., Ch'en, I. L., Korkina, O., Teng, X., Abbott, D., Cuny, G. D., Yuan, C., Wagner, G., Hedrick, S. M., Gerber, S. A., Lugovskoy, A., and Yuan, J. (2008) Identification of RIP1 kinase as a specific cellular target of necrostatins. *Nature chemical biology* **4**, 313-321
20. Cho, Y. S., Challa, S., Moquin, D., Genga, R., Ray, T. D., Guildford, M., and Chan, F. K. (2009) Phosphorylation-driven assembly of the RIP1-RIP3 complex regulates programmed necrosis and virus-induced inflammation. *Cell* **137**, 1112-1123
21. He, S., Wang, L., Miao, L., Wang, T., Du, F., Zhao, L., and Wang, X. (2009) Receptor interacting protein kinase-3 determines cellular necrotic response to TNF- α . *Cell* **137**, 1100-1111
22. Zhang, D. W., Shao, J., Lin, J., Zhang, N., Lu, B. J., Lin, S. C., Dong, M. Q., and Han, J. (2009) RIP3, an energy metabolism regulator that switches TNF-induced cell death from apoptosis to necrosis. *Science* **325**, 332-336
23. Sun, L., Wang, H., Wang, Z., He, S., Chen, S., Liao, D., Wang, L., Yan, J., Liu, W., Lei, X., and Wang, X. (2012) Mixed lineage kinase domain-like protein mediates necrosis signaling downstream of RIP3 kinase. *Cell* **148**, 213-227
24. Zhao, J., Jitkaew, S., Cai, Z., Choksi, S., Li, Q., Luo, J., and Liu, Z. G. (2012) Mixed lineage kinase domain-like is a key receptor interacting protein 3 downstream component of TNF-induced necrosis. *Proc Natl Acad Sci U S A* **109**, 5322-5327
25. Li, L., Thomas, R. M., Suzuki, H., De Brabander, J. K., Wang, X., and Harran, P. G. (2004) A small molecule Smac mimic potentiates TRAIL- and TNF- α -mediated cell death. *Science* **305**, 1471-1474
26. Wang, Z., Jiang, H., Chen, S., Du, F., and Wang, X. (2012) The mitochondrial phosphatase PGAM5 functions at the convergence point of multiple necrotic death pathways. *Cell* **148**, 228-243

27. Wang, H., Sun, L., Su, L., Rizo, J., Liu, L., Wang, L. F., Wang, F. S., and Wang, X. (2014) Mixed lineage kinase domain-like protein MLKL causes necrotic membrane disruption upon phosphorylation by RIP3. *Mol Cell* **54**, 133-146
28. Rodriguez, D. A., Weinlich, R., Brown, S., Guy, C., Fitzgerald, P., Dillon, C. P., Oberst, A., Quarato, G., Low, J., Cripps, J. G., Chen, T., and Green, D. R. (2016) Characterization of RIPK3-mediated phosphorylation of the activation loop of MLKL during necroptosis. *Cell Death Differ* **23**, 76-88
29. Cai, Z., Jitkaew, S., Zhao, J., Chiang, H. C., Choksi, S., Liu, J., Ward, Y., Wu, L. G., and Liu, Z. G. (2014) Plasma membrane translocation of trimerized MLKL protein is required for TNF-induced necroptosis. *Nat Cell Biol* **16**, 55-65
30. Chen, X., Li, W., Ren, J., Huang, D., He, W. T., Song, Y., Yang, C., Li, W., Zheng, X., Chen, P., and Han, J. (2014) Translocation of mixed lineage kinase domain-like protein to plasma membrane leads to necrotic cell death. *Cell Res* **24**, 105-121
31. Su, L., Quade, B., Wang, H., Sun, L., Wang, X., and Rizo, J. (2014) A plug release mechanism for membrane permeation by MLKL. *Structure* **22**, 1489-1500
32. Dondelinger, Y., Declercq, W., Montessuit, S., Roelandt, R., Goncalves, A., Bruggeman, I., Hulpiau, P., Weber, K., Sehon, C. A., Marquis, R. W., Bertin, J., Gough, P. J., Savvides, S., Martinou, J. C., Bertrand, M. J., and Vandenabeele, P. (2014) MLKL compromises plasma membrane integrity by binding to phosphatidylinositol phosphates. *Cell Rep* **7**, 971-981
33. Hildebrand, J. M., Tanzer, M. C., Lucet, I. S., Young, S. N., Spall, S. K., Sharma, P., Pierotti, C., Garnier, J. M., Dobson, R. C., Webb, A. I., Tripaydonis, A., Babon, J. J., Mulcair, M. D., Scanlon, M. J., Alexander, W. S., Wilks, A. F., Czabotar, P. E., Lessene, G., Murphy, J. M., and Silke, J. (2014) Activation of the pseudokinase MLKL unleashes the four-helix bundle domain to induce membrane localization and necroptotic cell death. *Proc Natl Acad Sci U S A* **111**, 15072-15077
34. Quarato, G., Guy, C. S., Grace, C. R., Llambi, F., Nourse, A., Rodriguez, D. A., Wakefield, R., Frase, S., Moldoveanu, T., and Green, D. R. (2016) Sequential Engagement of Distinct MLKL Phosphatidylinositol-Binding Sites Executes Necroptosis. *Mol Cell* **61**, 589-601
35. Huang, D., Zheng, X., Wang, Z. A., Chen, X., He, W. T., Zhang, Y., Xu, J. G., Zhao, H., Shi, W., Wang, X., Zhu, Y., and Han, J. (2017) The MLKL Channel in Necroptosis Is an Octamer Formed by Tetramers in a Dyadic Process. *Mol Cell Biol* **37**
36. Liu, S., Liu, H., Johnston, A., Hanna-Addams, S., Reynoso, E., Xiang, Y., Wang, Z. (2017) MLKL forms disulfide bond-dependent amyloid-like polymers to induce necroptosis. *Proc Natl Acad Sci U S A* (Accepted).
37. Vercammen, D., Beyaert, R., Denecker, G., Goossens, V., Van Loo, G., Declercq, W., Grooten, J., Fiers, W., and Vandenabeele, P. (1998) Inhibition of caspases increases the sensitivity of L929 cells to necrosis mediated by tumor necrosis factor. *J Exp Med* **187**, 1477-1485
38. Shindo, R., Kakehashi, H., Okumura, K., Kumagai, Y., and Nakano, H. (2013) Critical contribution of oxidative stress to TNF α -induced necroptosis downstream of RIPK1 activation. *Biochem Biophys Res Commun* **436**, 212-216
39. Zhang, Y., Su, S. S., Zhao, S., Yang, Z., Zhong, C. Q., Chen, X., Cai, Q., Yang, Z. H., Huang, D., Wu, R., and Han, J. (2017) RIP1 autophosphorylation is promoted by mitochondrial ROS and is essential for RIP3 recruitment into necrosome. *Nat Commun* **8**, 14329
40. Arner, E. S., and Holmgren, A. (2000) Physiological functions of thioredoxin and thioredoxin reductase. *Eur J Biochem* **267**, 6102-6109
41. Sies, H., Berndt, C., and Jones, D. P. (2017) Oxidative Stress. *Annu Rev Biochem*
42. Lu, J., and Holmgren, A. (2012) Thioredoxin system in cell death progression. *Antioxid Redox Signal* **17**, 1738-1747
43. Saitoh, M., Nishitoh, H., Fujii, M., Takeda, K., Tobiume, K., Sawada, Y., Kawabata, M., Miyazono, K., and Ichijo, H. (1998) Mammalian thioredoxin is a direct inhibitor of apoptosis signal-regulating kinase (ASK) 1. *EMBO J* **17**, 2596-2606

44. Liu, Y., and Min, W. (2002) Thioredoxin promotes ASK1 ubiquitination and degradation to inhibit ASK1-mediated apoptosis in a redox activity-independent manner. *Circ Res* **90**, 1259-1266
45. Matsui, M., Oshima, M., Oshima, H., Takaku, K., Maruyama, T., Yodoi, J., and Taketo, M. M. (1996) Early embryonic lethality caused by targeted disruption of the mouse thioredoxin gene. *Dev Biol* **178**, 179-185
46. Najafzadeh, A., Chen, H., and Yuan, J. (2017) Necroptosis and Cancer. *Trends Cancer* **3**, 294-301
47. Aaes, T. L., Kaczmarek, A., Delvaeye, T., De Craene, B., De Koker, S., Heyndrickx, L., Delrue, I., Taminiau, J., Wiernicki, B., De Groote, P., Garg, A. D., Leybaert, L., Grooten, J., Bertrand, M. J., Agostinis, P., Berx, G., Declercq, W., Vandenabeele, P., and Krysko, D. V. (2016) Vaccination with Necroptotic Cancer Cells Induces Efficient Anti-tumor Immunity. *Cell Rep* **15**, 274-287
48. Kirkpatrick, D. L., Kuperus, M., Dowdeswell, M., Potier, N., Donald, L. J., Kunkel, M., Berggren, M., Angulo, M., and Powis, G. (1998) Mechanisms of inhibition of the thioredoxin growth factor system by antitumor 2-imidazolyl disulfides. *Biochem Pharmacol* **55**, 987-994
49. Galmarini, C. M. (2006) Drug evaluation: the thioredoxin inhibitor PX-12 in the treatment of cancer. *Curr Opin Investig Drugs* **7**, 1108-1115
50. Ramanathan, R. K., Abbruzzese, J., Dragovich, T., Kirkpatrick, L., Guillen, J. M., Baker, A. F., Pestano, L. A., Green, S., and Von Hoff, D. D. (2011) A randomized phase II study of PX-12, an inhibitor of thioredoxin in patients with advanced cancer of the pancreas following progression after a gemcitabine-containing combination. *Cancer Chemother Pharmacol* **67**, 503-509
51. Ramanathan, R. K., Stephenson, J. J., Weiss, G. J., Pestano, L. A., Lowe, A., Hiscox, A., Leos, R. A., Martin, J. C., Kirkpatrick, L., and Richards, D. A. (2012) A phase I trial of PX-12, a small-molecule inhibitor of thioredoxin-1, administered as a 72-hour infusion every 21 days in patients with advanced cancers refractory to standard therapy. *Invest New Drugs* **30**, 1591-1596
52. Cong, L., Ran, F. A., Cox, D., Lin, S., Barretto, R., Habib, N., Hsu, P. D., Wu, X., Jiang, W., Marraffini, L. A., and Zhang, F. (2013) Multiplex genome engineering using CRISPR/Cas systems. *Science* **339**, 819-823

Figure Legends

Figure 1. Necrosulfonamide (NSA) crosslinks Cys86 of human MLKL to Cys32 of Trx1.

(A) Upper panel, domain structures of MLKL and NTD-DmrB. NTD, N-terminal domain; DmrB, dimerization domain. Middle panel, illustration of the Dox-inducible NTD-DmrB-FLAG expression system. Endogenous MLKL was knocked out in HeLa cells using CRISPR-Cas9, and Tet repressor (TetR) was stably expressed. Then NTD-DmrB-FLAG transgene under the control of a Dox-inducible promoter TetO2 was stably integrated into the genome. Dox, Doxycycline. Lower panel, cells were treated with or without Dox for 24 hours followed by anti-MLKL Western blotting. Endogenous MLKL was inactivated in NTD-DmrB-FLAG cells (lane 2 and 3). (B) Upper panel, chemical structures of NSA and a NSA variant, NSA-D1 (red asterisks denote Michael acceptor moieties needed for cysteine conjugation). Lower panel, NTD-DmrB-FLAG cells were treated with 5 μ M NSA or NSA-D1 for 16 hours prior to anti-FLAG Western blotting of whole cell extracts. Arrowhead near 55 kDa points to NSA-crosslinked NTD-DmrB product. (C) Cells stably expressing NTD-DmrB or NTD-C86S-DmrB mutant protein were treated with NSA followed by anti-FLAG Western blotting. (D) NTD-DmrB-FLAG cells were treated with NSA followed by FLAG-tag immunoprecipitation (FLAG-IP) and silver staining. The 55 kDa band was excised and sent for mass spectrometric analysis in which Trx1 peptides were identified. (E) Full-length HA-FLAG-MLKL and C86S mutant protein were ectopically expressed in HEK293T cells followed by NSA treatment. MLKL complexes were purified by FLAG-IP and analyzed by Western blotting. Arrowhead at 72 kDa points to the NSA-crosslinked MLKL-Trx1 product. (F) Upper panel, illustration of the HeLa:GFP-RIPK3:MLKL cell line. Dox-inducible GFP-RIPK3 and MLKL-HA-FLAG were stably integrated into the genome of the same HeLa cells used for NTD-DmrB-FLAG cells. Lower panel, HeLa:GFP-RIPK3:MLKL cells with or without ectopic HA-Trx1 expression were treated with Dox and NSA followed by FLAG-IP and Western blotting. Both endogenous Trx1 and HA-Trx1 were conjugated to MLKL by NSA (lane 4). (G) A panel of HA-tagged mutant Trx1 proteins were ectopically expressed in HeLa:GFP-RIPK3:MLKL cells followed by Dox and NSA treatment. FLAG-IP products were analyzed by Western blotting. In HA-Trx1-CS2 mutant, both C32 and C35 were mutated to serine.

Figure 2. Recombinant Trx1 interacts with MLKL in a signal-dependent manner.

(A) Purified HA-Trx1-6XHis was immobilized to nickel-agarose beads, and incubated with whole cell extracts from HeLa:GFP-RIPK3:MLKL cells. MLKL binding was analyzed by anti-FLAG Western blotting. (B) Western blot analysis of DMSO- or T/S/Z-treated HT-29 cell extracts. TNF- α (T); S, Smac-mimetic (S); Z-VAD-FMK (Z). P-MLKL, antibody against phospho-Ser358 of human MLKL. (C) Purified Trx1 proteins (wild-type, C35S single mutant, and C32S-C35S (CS2) double mutant) were immobilized to nickel beads, and incubated with either DMSO- or T/S/Z-treated HT-29 whole cell extracts. MLKL binding was analyzed by anti-MLKL Western blotting.

Figure 3. Trx1 reduces MLKL disulfide bond formation to inhibit MLKL polymerization.

(A) HeLa:GFP-RIPK3:MLKL cells were treated with Dox for 24 hours followed by DMSO or T/S/Z treatment for 8 hours. Cell extracts were analyzed by Western blotting using indicated antibodies. (B) Cells were treated as in (A) and cell extracts were analyzed by non-reducing SDS-PAGE gel. In lane 3 and 4, cell extracts were incubating with 10 mM β -mercaptoethanol (β -ME) at 30°C for 30 minutes. Western blotting was performed with antibodies against phospho-S358 of MLKL (upper panel) or FLAG-tag (lower panel). (C) Cells were treated as in (A) and cell extracts were analyzed by semi-denaturing detergent agarose gel electrophoresis (SDD-AGE). In lane 3 and 4, cell extracts were incubating with 5 mM dithiothreitol (DTT) at 30°C for 30 minutes. (D) *In vitro* MLKL polymerization assay. Recombinant GST-NTD-FLAG protein was incubated at 4°C (Lane 1) or 37°C (lane 2) for 16 hours. Lane 2 sample was further incubated with 5 mM DTT at 37°C for 30 minutes and loaded in lane 3. (E) Increasing amounts of wild-type Trx1 or CS2 mutant (3 μ M, 10 μ M and 30 μ M) were mixed with 5 μ M recombinant GST-NTD-FLAG and incubated at 37°C for 16 hours. In lane 8, 1 mM DTT was used. The samples were then separated by non-reducing SDS-PAGE (upper panel) or standard SDS-PAGE (lower panel). (F) Samples were treated

as in (E) and analyzed by SDD-AGE (upper panel). Protein loading was visualized with Coomassie Blue staining (lower panel).

Figure 4. ShRNA-mediated Trx1 knockdown promotes MLKL polymerization and sensitizes cells to necroptosis.

(A) Lentiviruses encoding Dox-inducible shRNA against Trx1 were transduced into HeLa:GFP-RIPK3:MLKL cells to establish shTrx1 cell line. Cells were treated with Dox for 72 hours and Western blotting was performed to compare Trx1, RIPK3, and MLKL protein levels in parental cells versus shTrx1 cells. (B) Cells were treated with or without Dox for 72 hours and cell extracts were analyzed by non-reducing SDS-PAGE. (C) Cells were treated with or without Dox for 72 hours and cell extracts were analyzed by SDD-AGE. Asterisk denotes a non-specific signal. (D) Cells were treated with or without Dox for 72 hours and cell survival was quantified by CellTiter-Glo assay. All cells were co-treated with Z-VAD-FMK to protect against apoptosis. Triplicate samples were used for each treatment. Data are presented as mean \pm SD (** P < 0.01, Student's t test). (E) Working model. Trx1 maintains MLKL in a reduced state to prevent spontaneous disulfide bond formation and necrosome recruitment. (F) Cells were treated with Dox for 72 hours followed by NSA treatment for an additional 16 hours. MLKL complexes were purified by FLAG-IP and analyzed by Western blotting. Arrowhead points to the NSA-crosslinked MLKL-Trx1 product. (G) Cells were treated with Dox and Z-VAD-FMK for 72 hours followed by another 16 hours of treatment with T/S/Z or T/S/Z plus NSA. Cell death was quantified by CellTiter-Glo assay. Triplicate samples were used for each treatment. Data are presented as mean \pm SD (** P < 0.01, Student's t test).

Figure 5. Inhibition of Trx1 activity with PX-12 induces necrosome formation and necroptosis in HeLa:GFP-RIPK3:MLKL cells.

(A) HeLa:GFP-RIPK3:MLKL cells were treated with DMSO, Dox or Dox plus NSA for 24 hours, followed by PX-12 (3-30 μ M) or T/S/Z treatment for another 16 hours. Cell survival was quantified by CellTiter-Glo assay. Z-VAD-FMK (20 μ M) was included in all treatments to prevent apoptosis. Triplicate samples were used for each treatment. Data are presented as mean \pm SD (P < 0.005, One-Way ANOVA analysis). (B) Cells were treated as in (A) followed by SYTOX Green and Hoechst staining. Scale bar represents 20 μ m. (C) HeLa:GFP-RIPK3:MLKL cells were induced with Dox for 24 hours followed by PX-12 (10 μ M) or T/S/Z treatment for 6 hours. Whole cell extracts were subjected to FLAG-IP and Western blot analysis. (D) Cells were treated as in (C) and cell extracts were analyzed by non-reducing SDS-PAGE with anti-FLAG (left panel) or anti-pS358 MLKL antibodies (right panel). (E) Cells were treated as in (C) and cell extracts were analyzed by SDD-AGE. (F) Working model. Inhibition of Trx1 by PX-12 increases MLKL disulfide bond formation, which promotes its recruitment into the necrosome to trigger necroptosis.

Figure 6. Inhibition of Trx1 activity with PX-12 induces RIPK3-independent MLKL polymerization and necroptosis in NTD-DmrB cells.

(A) Left panel, illustration of Dimerizer induced NTD-DmrB polymerization. Right panel, NTD-DmrB-FLAG cells were treated with DMSO, Dox or Dox plus NSA for 24 hours, followed by PX-12 (1-10 μ M) or Dimerizer treatment for another 16 hours. Cell survival was quantified by CellTiter-Glo assay. Z-VAD-FMK (20 μ M) was included in all treatments to prevent apoptosis. Triplicate samples were used for each treatment. Data are presented as mean \pm SD (P < 0.005, One-Way ANOVA analysis). (B) NTD-DmrB-FLAG cells were treated as in (A), followed by SYTOX Green and Hoechst staining. Scale bar represents 20 μ m. (C-D) NTD-DmrB-FLAG cells were induced with Dox for 24 hours followed by 10 μ M PX-12/Z or Dimerizer/Z treatment for 6 hours. Cell extracts were analyzed by non-reducing SDS-PAGE (C) and SDD-AGE (D), respectively. (E) Working model. In some cells, expressed MLKL isoforms do not contain the full length auto-inhibitory C-terminal kinase-like domain. Inhibition of Trx1 in these cells can directly induce disulfide bond-dependent MLKL polymer formation independent of RIPK3 to promote necroptosis.

Figure 1

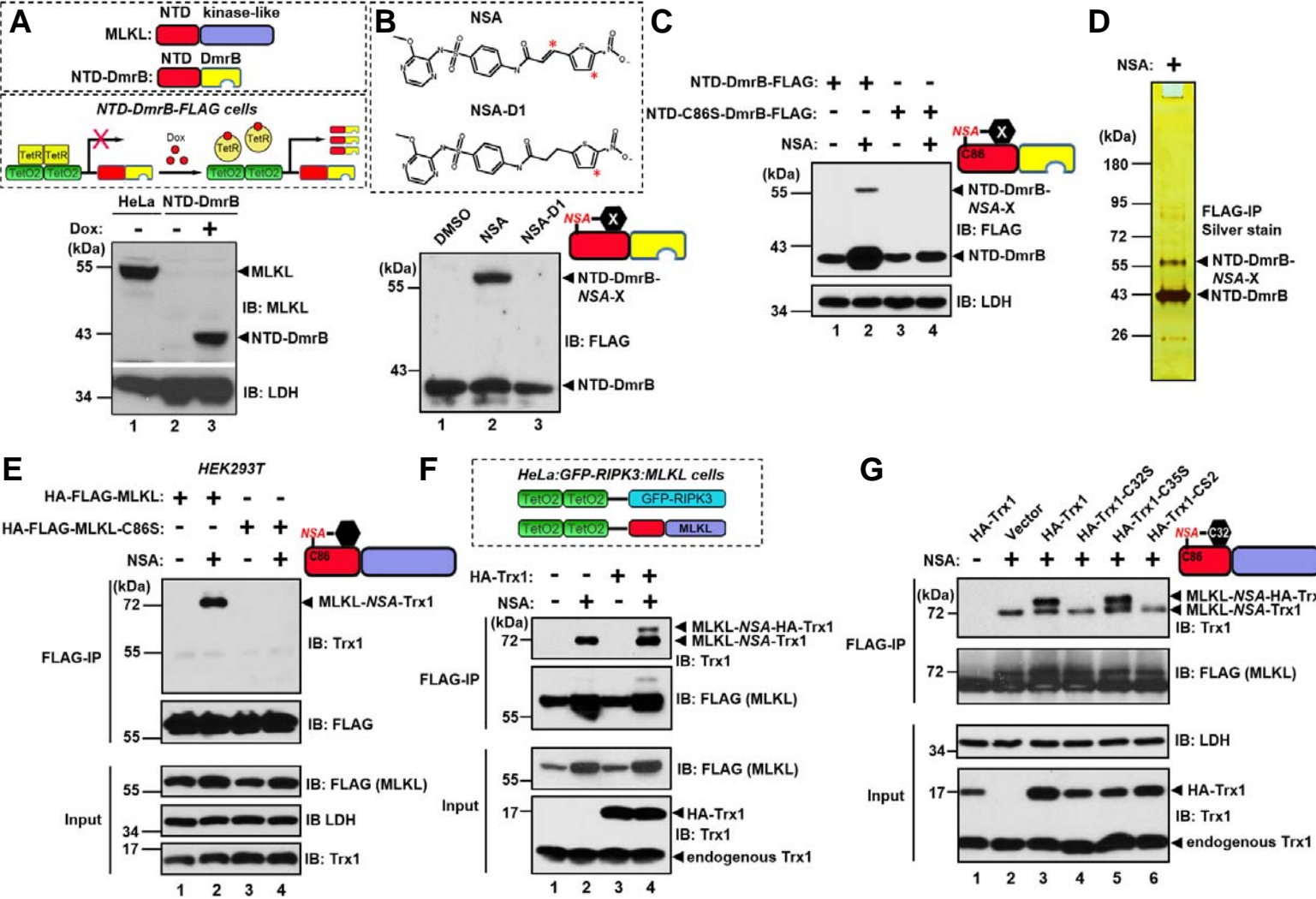


Figure 2

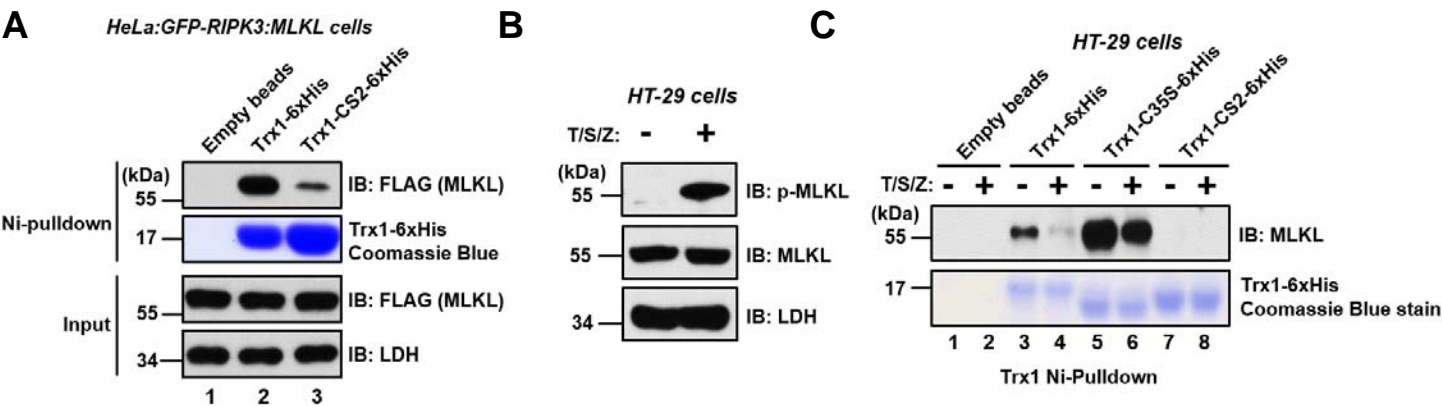


Figure 3

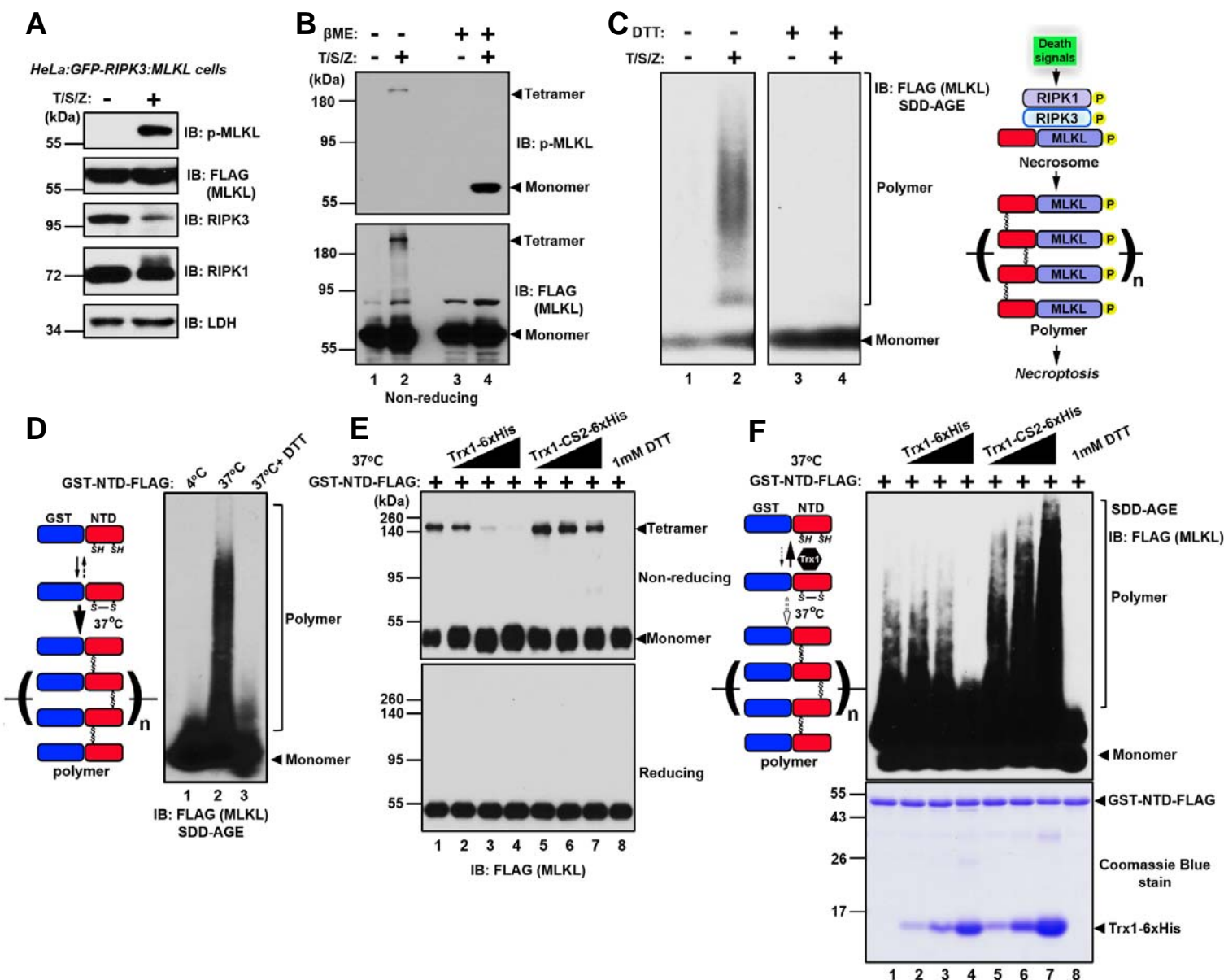


Figure 4

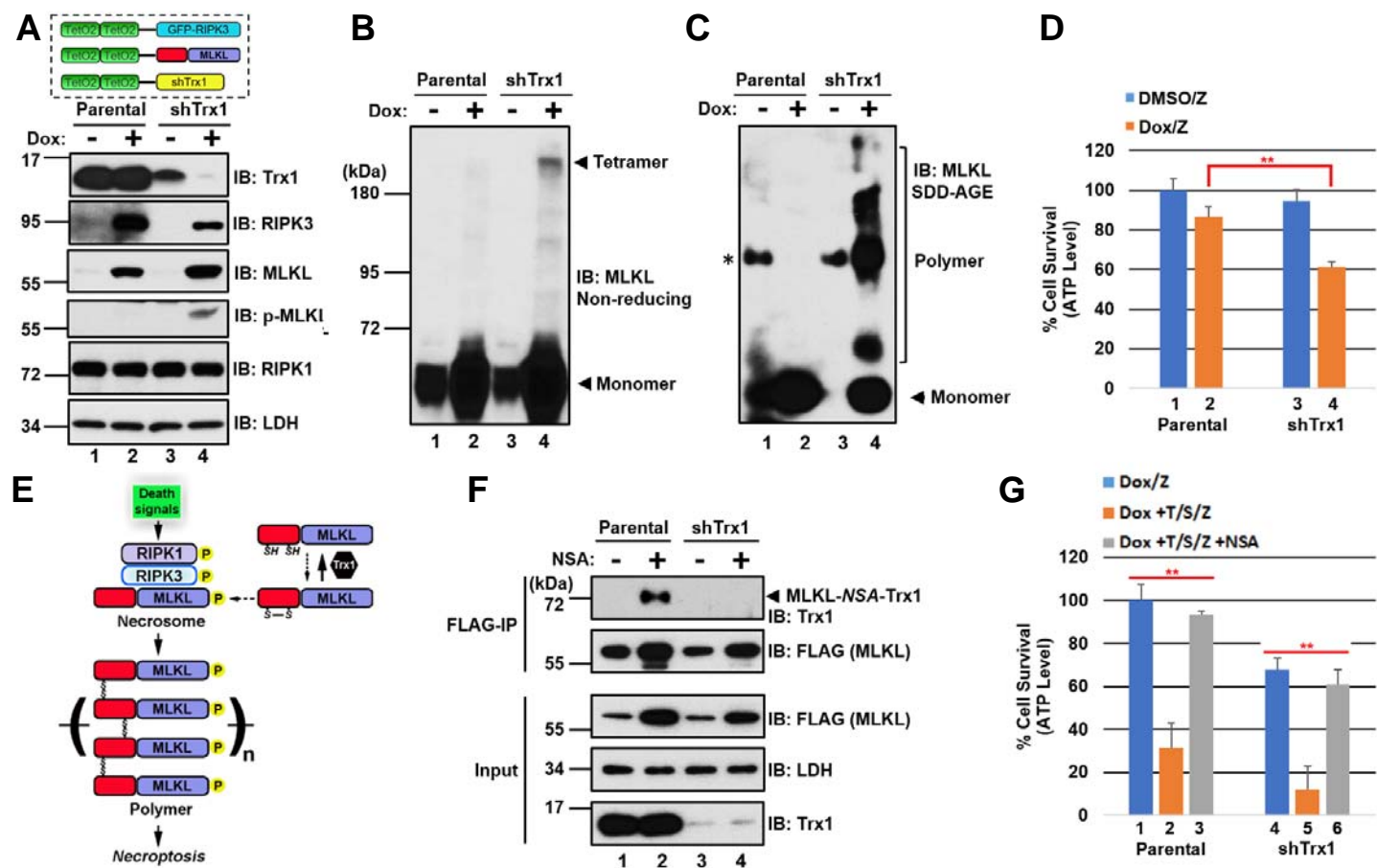


Figure 5

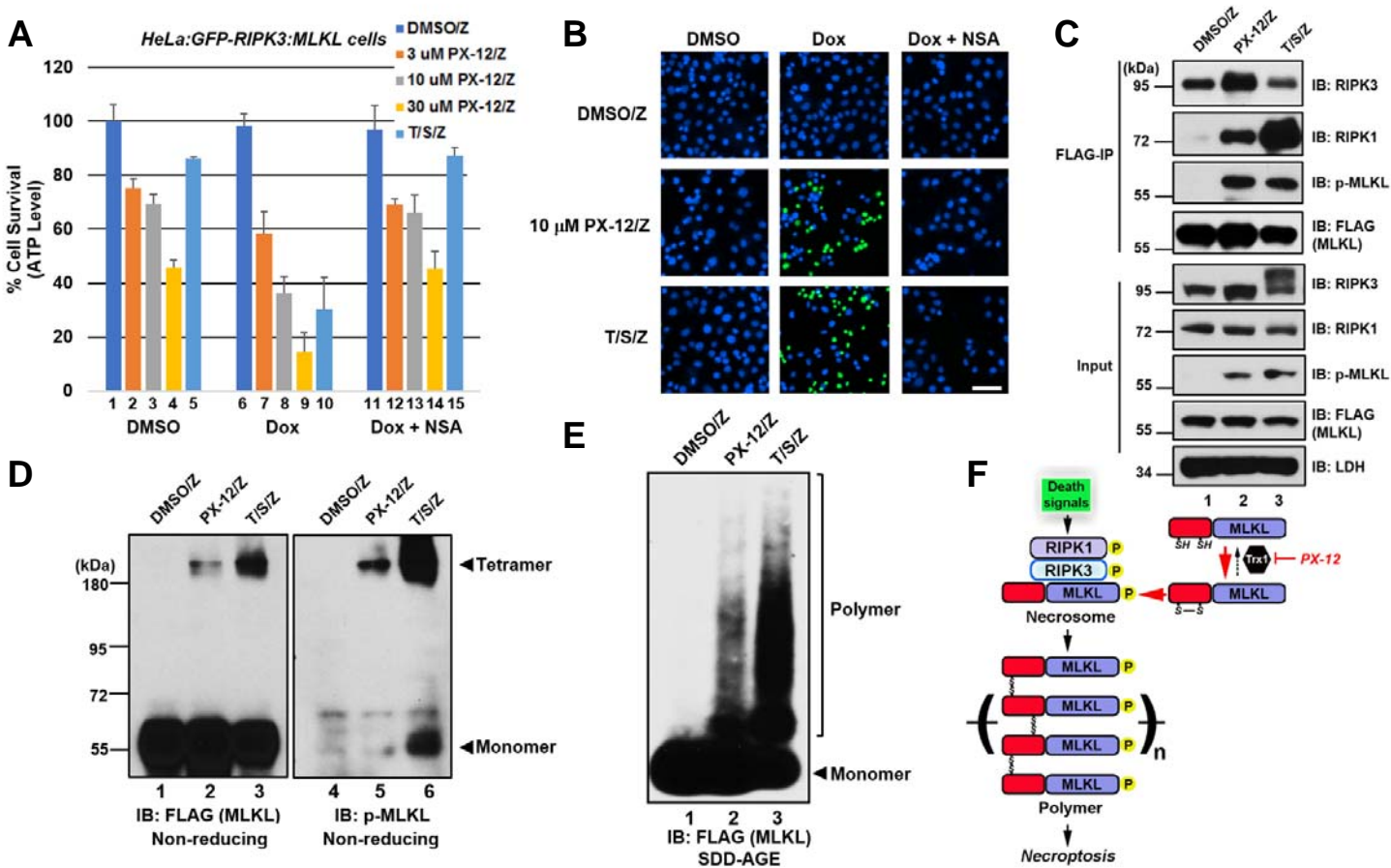
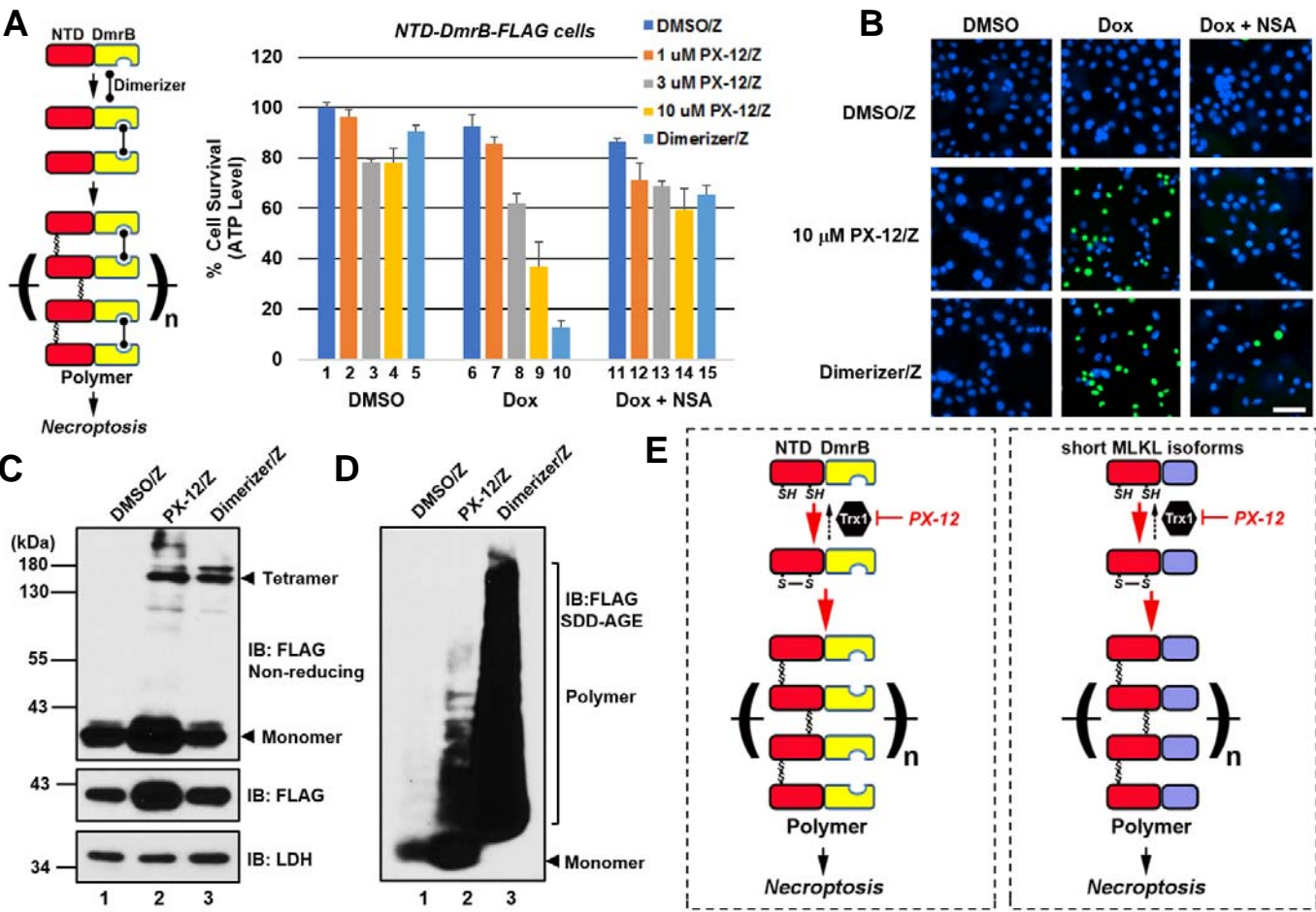


Figure 6



Thioredoxin-1 actively maintains the pseudokinase MLKL in a reduced state to suppress disulfide bond-dependent MLKL polymer formation and necroptosis

Eduardo Reynoso, Hua Liu, Lin Li, Anthony L. Yuan, She Chen and Zhigao Wang

J. Biol. Chem. published online September 6, 2017

Access the most updated version of this article at doi: [10.1074/jbc.M117.799353](https://doi.org/10.1074/jbc.M117.799353)

Alerts:

- [When this article is cited](#)
- [When a correction for this article is posted](#)

[Click here](#) to choose from all of JBC's e-mail alerts